


Article

Coadsorption Interfered CO Oxidation over Atomically Dispersed Au on *h*-BN

Xin Liu ^{*} , Xin Zhang and Changgong Meng ^{*}

State Key Laboratory of Fine Chemicals, Department of Chemistry, Dalian University of Technology, Dalian 116024, China; xin0123@mail.dlut.edu.cn

^{*} Correspondence: xliu@dlut.edu.cn (X.L.); cgmeng@dlut.edu.cn (C.M.)

Abstract: Similar to the metal centers in biocatalysis and homogeneous catalysis, the metal species in single atom catalysts (SACs) are charged, atomically dispersed and stabilized by support and substrate. The reaction condition dependent catalytic performance of SACs has long been realized, but seldom investigated before. We investigated CO oxidation pathways over SACs in reaction conditions using atomically dispersed Au on *h*-BN (AuBN) as a model with extensive first-principles-based calculations. We demonstrated that the adsorption of reactants, namely CO, O₂ and CO₂, and their coadsorption with reaction species on AuBN would be condition dependent, leading to various reaction species with different reactivity and impact the CO conversion. Specifically, the revised Langmuir–Hinshelwood pathway with the CO-mediated activation of O₂ and dissociation of cyclic peroxide intermediate followed by the Eley–Rideal type reduction is dominant at high temperatures, while the coadsorbed CO-mediated dissociation of peroxide intermediate becomes plausible at low temperatures and high CO partial pressures. Carbonate species would also form in existence of CO₂, react with coadsorbed CO and benefit the conversion. The findings highlight the origin of the condition-dependent CO oxidation performance of SACs in detailed conditions and may help to rationalize the current understanding of the superior catalytic performance of SACs.



Citation: Liu, X.; Zhang, X.; Meng, C. Coadsorption Interfered CO Oxidation over Atomically Dispersed Au on *h*-BN. *Molecules* **2022**, *27*, 3627. <https://doi.org/10.3390/molecules27113627>

Academic Editor: Stefano Falcinelli

Received: 23 May 2022

Accepted: 3 June 2022

Published: 5 June 2022

Publisher's Note: MDPI stays neutral with regard to jurisdictional claims in published maps and institutional affiliations.



Copyright: © 2022 by the authors. Licensee MDPI, Basel, Switzerland. This article is an open access article distributed under the terms and conditions of the Creative Commons Attribution (CC BY) license (<https://creativecommons.org/licenses/by/4.0/>).

Keywords: single atom catalysis; Au; CO oxidation; reaction conditions; *h*-BN; first principles

1. Introduction

Single atom catalysis is emerging and growing as a new frontier in catalysis [1,2]. Similar to the metal centers in enzymes and transition metal complexes in biocatalysis and homogeneous catalysis, the transition metal species in SACs are charged and atomically dispersed on the support [3,4]. In reaction conditions, the thermodynamics-driven adsorption and reaction of substrates would change the oxidation state [5] and coordination of metal species drastically [6], and may stabilize metal species in an atomically dispersed form or promote their aggregation or redispersion [7]. This feature of transition metal species in reaction conditions were reported for Au [8–12], Pd [13], and Rh [14]-based SACs, etc. Apart from the potential aggregation/redispersion of metal species, the adsorption/coadsorption of the substrate may also impact the thermodynamics and kinetics for the evolution of reaction species and may lead to a switch of the pathways for substrate conversion with reactions conditions, such as temperature, substrate concentrations (partial pressures), [15–19] etc. For these complexities, the impact of the reaction condition to active sites and active species was seldom investigated [19].

Low temperature catalytic oxidations of CO oxidation to CO₂ are the key components in many industrial chemical processes, such as the water–gas–shift reaction [20], CO preferential oxidation in H₂ rich stream (CO-PROX) [21], exhaust gas control [22], etc. Apart from the practical applications, CO oxidation is widely used as a prototypical reaction for fundamental investigations [23] and it is also the first catalytic reaction realized on Pt₁/FeO_x [24]. Continuous efforts have been made to develop novel CO oxidation

catalysts that are efficient at low temperatures [22]. Among transition metals used for CO oxidation, Au is special, as it is chemically inert in the bulk phase, and is highly active when is downsized to a sub-nano scale [25,26]. Since the supported Au nanoparticles were found active for CO oxidation in the 1980s, tremendous efforts have been put to understand the active species and mechanism pathways for the Au-catalyzed CO oxidation in operating conditions [26]. For many of these cases, the charged Au atoms, formed dynamically in reaction conditions, were proposed to be the active sites [5,10–12,19,27,28]. Furthermore, it has been demonstrated that Au SACs are highly active for many reactions [29], such as the water–gas–shift [27], methanol steam reforming [30], epoxidation of ethylene, [31] acetylene hydrochlorination [32], selective hydrogenation [33], ethanol dehydrogenation reactions [34], CO oxidation [11,19,35–39], etc.

Hexagonal boron nitride (*h*-BN) is a 2D material with graphene-like planar structure [40]. Defects, such as vacancies, etc., that are capable of modulating electronic properties of *h*-BN, can be created by electron beam irradiation, solvent and gas exfoliation, ball milling [41,42], etc. The metal/defective *h*-BN interaction stabilizes the metal species and tailors their reactivity [43–49]. Several *h*-BN-supported SACs have been proposed effective for reactions of practical interest, such as the electroreduction of N₂ and CO₂ [47–50], hydrogenation of Cinnamaldehyde [51], dehydrogenation of light alkanes [52] and CO oxidation [53,54] etc. However, the active site and active species in reaction conditions for these processes have not been addressed.

Recently, we theoretically explored the reaction network for CO oxidation over Pd₁ and Fe₁ SACs on graphene and highlighted the vital role of the thermostability of reaction species in determining CO conversion and reaction pathways [55,56]. In this work, we focus on CO oxidation over AuBN to highlight the impact of coadsorbed substrates to the formation and evolution of surface species on SACs in reaction conditions with extensive first-principles-based calculations. We expect the finding would be helpful for the discovery of new reaction pathways and a rationalized understanding to the observed superior performance of SACs.

2. Theoretical Methods

All the first-principles-based calculations were performed using the GGA-PBE functional [57] with the DSPP pseudopotential [58] and DNP basis set [59], as implemented in DMol³ [60,61]. CO oxidation over AuBN was investigated in a 6 × 6 supercell of *h*-BN. The Brillouin Zone was sampled with a Γ -centered 4 × 4 × 1 *k*-point grid [62]. The global orbital cutoff was set as 4.50 Å and the convergence criterion for energy and forces were 3 × 10^{−4} eV and 5 × 10^{−2} eV/Å, respectively. The transition states (TSs) were determined with synchronous transition methods, and further optimized and confirmed with frequency analysis, so that the only negative frequency is on the bond formation/dissociation direction [63]. The Hirshfeld scheme was adapted for population analysis [64]. With the above setup, the bulk lattice parameter of face-center-cubic Au and *h*-BN were calculated as 4.20 and 2.52 Å, respectively [65,66].

The formation free energy of a reaction species with stoichiometry of Au(CO)_x(O₂)_y over AuBN, under CO oxidation conditions, was calculated as: $\Delta G = G_{Au(CO)_x(O_2)_y} - E_{Au} - G_{BN} - x \times G_{CO} - y \times G_{O_2} + z \times G_{CO_2}$. Here, *x*, *y* and *z* are the stoichiometry for CO, O₂ and CO₂ involved in the formation of Au(CO)_x(O₂)_y, respectively, $G_{Au(CO)_x(O_2)_y}$ and G_{BN} are the free energy of Au(CO)_x(O₂)_y and B-vacancy *h*-BN, respectively, E_{Au} is the energy of an Au atom, G_{CO} and G_{O_2} are free energy of gas molecules calculated as $G_{gas}(T, p) = E_{gas}^e + \Delta\mu_{gas}(T, p^0) + k_B T \ln\left(\frac{p}{p^0}\right)$, where E_{gas}^e is the calculated total energy of the gas molecule and $\Delta\mu_{gas}(T, p^0)$ is derived from calculated partition functions of the gas molecule. The reaction conditions described by *T*, *p* were previously used to characterize the performance of SACs in CO oxidation [67].

3. Results and Discussions

3.1. Thermodynamics Analysis of Potential Reaction Species

We firstly evaluated the formation of Gibbs free energies (ΔG) of all the potential reactants at various temperatures (T) at $P_{\text{CO}}:P_{\text{O}_2} = 1:20$ and $P_{\text{CO}} = 0.01$ atm (Figure 1), which are commonly used to characterize the CO oxidation performance of a catalyst [67].

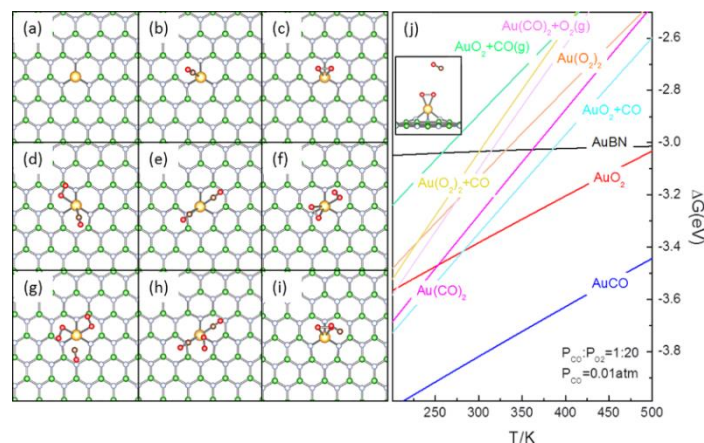


Figure 1. The calculated atomic structures (a–i) and temperature dependence of ΔG (j) for the potential reaction species formed over AuBN in CO oxidation. Please see the context for the notation of structures. ΔG was calculated with respect to B-vacancy on *h*-BN, Au atom at $P_{\text{CO}} = 0.01$ atm and $P_{\text{CO}}/P_{\text{O}_2} = 1:20$. The inset in (j) is the sideview of (i). In (a–i), the B, N, C, O and Au atoms are in green, light blue, brown, red and gold, respectively.

The calculated binding energy (E_b) of the Au atom on the B-vacancy of *h*-BN (AuBN, Figure 1a) in a triplet ground state is -3.54 eV and is comparable to calculated (-2.90 eV), previous theoretical (-3.03 eV) [68] and experimental results of bulk Au (-3.81 eV) [69], suggesting AuBN would be plausible over other potential Au deposition structures [52,53]. Considering the poor E_b of the Au atom (-0.11 and -0.10 eV, respectively, on top of N and B atoms on pristine *h*-BN), the outward diffusion of Au from AuBN would be highly endothermic (>3 eV), so it is hard to expect that the Au atom would diffuse away. In AuBN, the Au–N distances are ~ 2.08 Å and Au is $0.45 |e|$ positively charged. These are in excellent agreement with the reported X-ray photoelectron spectroscopy of Au SACs [24,34,35,70], transition metal SACs on *h*-BN and Au/*h*-BN nanocomposites, where the Au and TM atoms are confirmed to be positively charged as reaction centers [41,51,71]. The thermodynamics data (Figure 1j) demonstrated that CO adsorbed on AuBN (AuCO, Figure 1b, $E_{\text{ad}} = -1.38$ eV) is the most plausible at temperatures from 200 to 500 K. In AuCO, Au is $0.36 |e|$ positively charged, and C–O bond is in the direction nearly reverse to one of the Au–N bonds at Au–C distance of 1.93 Å and is slightly stretched (1.16 Å). As for the adsorption of O_2 (AuO_2 , Figure 1c, $E_{\text{ad}} = -0.90$ eV), the O–O bond is elongated to 1.33 Å, parallel to the *h*-BN surface, and is nearly vertical to one of the N–Au bonds, forming an undercoordinated octahedral. Au is $0.53 |e|$ positively charged and the spin density is localized on Au and O atoms. ΔG of other potential species (Figure 1d–i) were also collected (Figure 1j). ΔG of AuO_2 and the coadsorption of CO and O_2 ($\text{AuO}_2 + \text{CO}$, Figure 1d, $E_{\text{ad}} = -1.49$ eV) stand right above that of AuCO, are negative from 250 to 500 K and intersect each other at ~ 280 K, demonstrating that $\text{AuO}_2 + \text{CO}$ may form from AuCO via coadsorption with O_2 or by an exchange of adsorbates. ΔG of other coadsorption species, such as coadsorption of 2 CO ($\text{Au}(\text{CO})_2$, Figure 1e), 2 O_2 ($\text{Au}(\text{O}_2)_2$, Figure 1f) and the van de Waals complexes formed between adsorbed O_2/CO and gaseous molecules, such as $\text{Au}(\text{O}_2)_2 + \text{CO}(\text{g})$, $\text{Au}(\text{CO})_2 + \text{O}_2(\text{g})$ and $\text{AuO}_2 + \text{CO}(\text{g})$ (Figure 1g–i), etc., are much higher in ΔG than those for AuO_2 , AuCO and $\text{AuO}_2 + \text{CO}$ (Figure 1j). Though these species may potentially exist, their coverage would be much lower than those for the AuCO, AuO_2 and $\text{AuO}_2 + \text{CO}$, and they would evolve into these more stable species by adsorbate desorption

or exchange. Our results (Figure 1) clearly indicate that AuCO (Figure 1b) is the most plausible reaction species in the 200–500 K temperature range, under CO oxidation conditions. We also investigated the impact of CO and O₂ chemical potential on the relative stability in terms of the ΔG of these reaction species by varying the CO and O₂ partial pressure in the range of 0.01–0.2 atm in the same temperature interval. Though the calculated values of ΔG of these identified major reactants, namely AuCO, AuO₂, AuO₂ + CO and Au(CO)₂ (Figure 1b–e) may shift due to the variation of reaction conditions, AuCO is still the most plausible, considering that the ΔG of AuO₂ and AuO₂ + CO remain right above that of AuCO. This is in reasonable agreement with the experimental finding that the active reaction species in SAC-catalyzed CO oxidation all originate from positively charged or even oxidized metal atoms [72–75]. We also investigated the potential impact of van der Waals interactions on the relative stability of these species within the same temperature and partial pressure range, and yielded exactly the same finding. The calculated stretching frequency of AuCO (Figure 1b) is slightly redshifted from that of gaseous CO, i.e., from 2143 cm⁻¹ to 2040 cm⁻¹, and further shifted to 2115 cm⁻¹ in AuO₂ + CO (Figure 1d). The calculated CO stretching frequencies correlate well with the calculated charge on Au in AuBN, AuCO and AuO₂ + CO, confirming the positively charged nature of the Au atom in AuBN. Similar redshifts of the C = O stretching frequency have been reported for CO oxidation over Au and Pd-based SACs and nanoparticles catalysts [20,74–77]. Based on the consistent evidence for the positively charged nature of AuBN (Figure 1a, AuBN), we moved further to investigate its performance in CO oxidation.

3.2. Revised LH Pathway for CO Oxidation over AuBN

Based on experimental and theoretical results, several pathways have been proposed for the CO oxidation over SACs [22], which can be classified into two kinds according to the involvement of support during the reaction. Pristine *h*-BN is chemically inert to CO and O₂. As shown in Figure 1a, the proposed AuBN has the B-vacancy on *h*-BN fully passivated, there is no other defect at the chemical bond distance from Au to stabilize CO, O₂ or other reaction species. Therefore, the pathways that require support or defects on the support for stabilization and activation of CO or O₂, and formation and stabilization of reaction species, such as the Mars-van-Krevelen type pathway and its variants that requires support oxygen to initiate [24,70], support-promoted CO oxidation that needs support to stabilize reactants [78], etc., are not applicable on AuBN. Another kind of CO oxidation pathway inherits the merit of Langmuir–Hinshelwood (LH) and Eley–Rideal (ER) type pathways derived from bulk metals [79,80], involving the adsorption and activation of one reactant (ER), either CO or O₂, or both (LH) only on the metal species. We recently investigated CO oxidation over the defect-stabilized Fe and Pd SACs on graphene and demonstrated that the coadsorption of CO and O₂ would be more plausible on these SACs over van de Waals complexes and the coadsorption of 2 CO to initiate CO oxidation on ER type pathways. Thus, it would be a major reaction species with a population superior to those van de Waals complexes and is the active species to initiate CO oxidation [55,56,81]. The calculated thermodynamics stability of reaction species on AuBN (Figure 1j) also demonstrated such a trend that AuO₂ + CO is more plausible than AuO₂ + CO(g) and Au(CO)₂, though AuCO is the most plausible species in reaction conditions. This AuO₂ + CO (Figure 1d) satisfies the requirements to initiate reaction on LH type pathways that both O₂ and CO adsorb on AuBN and get activated for reactions. The first reported pathway of the LH type involves coadsorbed CO-assisted O₂ activation through the formation and dissociation of peroxide (OCOO) species on the metal center (revised Langmuir–Hinshelwood pathway, rLH), and was originally proposed by Iglesia et al., and was then adapted as the pathway for the CO and ethylene oxidation over Au SAC [31,39,82]. We then started with the rLH pathway from AuO₂ + CO (LH-IS1, Figure 2a).

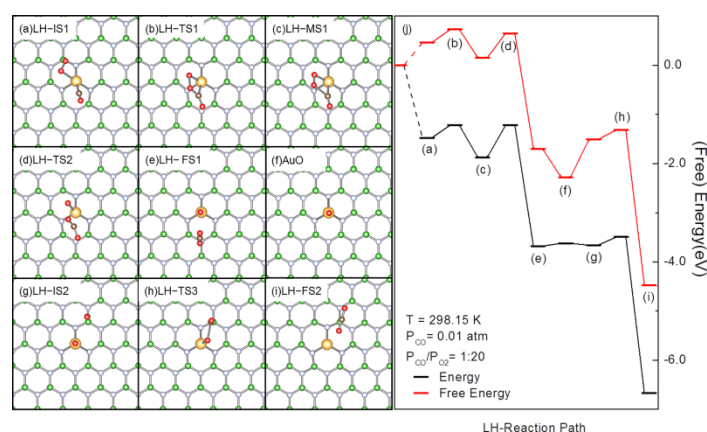


Figure 2. Optimized structures of the reaction species involved, including reaction intermediates, transition states and products (a–i), and (free) energy profiles (j) for CO oxidation over AuBN through the rLH pathway. In (a–i), the B, N, C and Au atoms are in green, light blue, brown and gold, respectively. In (j), the bracketed letters correspond to the structures shown in (a–i).

The elementary steps on the rLH pathway for CO oxidation were investigated (Figure 2). The E_{ad} for $AuO_2 + CO$ (LH-IS1, Figure 2a, the same as Figure 1d) is -1.48 eV. In LH-IS1, Au-C(CO) and Au-O(O₂) are both in directions reverse to Au-N bonds. Though the E_{ad} of CO and O₂ are significant, they are repulsive to each other, making ΔG for the LH-IS1 formation (at 298.15 K, $P_{CO} = 0.01$ atm, $P_{CO}/P_{O_2} = 1:20$) 0.46 eV higher than that of AuCO (Figure 1b). Considering the large exothermicity for the formation of LH-IS1 (~ -3.00 eV), LH-IS1 may exist but with a smaller population. The variation of ΔG from AuCO to LH-IS1 also suggests that CO in $AuO_2 + CO$ (LH-IS1) would be active for subsequent reactions [76]. Driven by the electrostatic interaction between O(O₂) (-0.06 |e|) and C(CO) ($+0.15$ |e|), the O(O₂) atom moves to interact with C(CO). By crossing a transition state (LH-TS1, Figure 2b) with energy and free energy barriers of 0.26 and 0.27 eV, respectively, a peroxide intermediate (LH-MS1, Figure 2c) is formed. The newly formed C-O bond stabilizes the reaction product and makes the formation of LH-MS1 slightly exothermic ($\Delta G = -0.31$ eV) with respect to LH-IS1. In LH-MS1, the O-O distance is elongated to 1.51 Å and is typical for O-O bonds in peroxides [83]. The C=O stretching frequency in LH-MS1 was calculated as 1748 cm⁻¹, which falls in the higher range of experimentally reported values [73–75]. Due to the instability of the peroxide O-O bond, charge reorganization may take place within LH-MS1 for passing a TS (LH-TS2, Figure 2e) to form a CO₂ molecule (LH-FS1, Figure 2f). This tendency for breaking the O-O bond and reorganizing the structure to form CO₂ is well evidenced by the change of C=O distance from 1.72 to 1.18 Å, and the elongation of O-O and Au-C distances from 1.51 and 2.11 Å, respectively, to 3.35 and 4.27 Å, respectively. Charge transfer to C and 2 O(O₂) atoms also takes place simultaneously. The calculated Hirshfeld charges on the C and 2 O(O₂) increase from 0.09, -0.18 , -0.05 |e|, respectively, in LH-MS1 to 0.10, -0.10 and -0.30 |e|, respectively, in LH-TS2. This charge transfer is further enhanced in LH-FS1, where the charges on C, O(CO₂), O(Au) and Au are 0.28, -0.15 , -0.30 and 0.56 |e|, respectively, implying the oxidation of Au in this process and the weak binding of CO₂ to the Au = O center. This is in agreement with the calculated E_{ad} of CO₂ in LH-FS1 of only -0.07 eV. The further desorption of CO₂ leads to the formation of AuO (Figure 2f), which is more thermodynamically stable than LH-FS1. AuO will then form a van de Waals complex with gaseous CO (LH-IS2, Figure 2g). The calculated ΔE and ΔG between LH-FS1 and LH-IS2 are only 0.02 and 0.19 eV, respectively. The electrostatic interaction between C(CO) ($+0.06$ |e|) and O(Au) (-0.30 |e|) stabilizes LH-IS2 and initiates the subsequent reaction with charge transfer from the 5σ of CO to the π* on O(Au) for the reduction of Au. CO moves towards O(Au) in this process to reach the transition state (LH-TS3, Figure 2h), where the C-O(Au) distance decreases to 1.90 Å and the calculated Hirshfeld charge on C and O(Au) changes to 0.06 and -0.26 |e|, respectively, indicating a

charge transfer from CO to O for the formation of the C=O bond. By crossing the energy barrier of 0.17 eV (LH-TS3), another CO₂ is formed (LH-FS2, Figure 2i). CO₂ desorption from AuCO₂ would be easy even at a low temperature, as the calculated E_{ad} of CO₂ is only -0.07 eV and thus closes the catalytic cycle for CO oxidation along the rLH pathway.

3.3. Interference of the Coadsorption of CO or O₂ to CO Oxidation

LH-MS1 is an important intermediate on the rLH pathway with a dissociation free energy barrier of 0.51 eV at 298.15 K when $P_{\text{CO}} = 0.01$ atm and $P_{\text{CO}}/P_{\text{O}_2} = 1:20$. Considering the high barrier for dissociation and a small barrier for formation, LH-MS1 would be one of the major reaction species [55]. A careful inspection of the structure shows that Au in LH-MS1 is not fully coordinated in a penta coordinated environment, implying potential coadsorption and further reactions with CO or O₂ (Figure 3). The calculated E_{ad} for CO coadsorption with LH-MS1 (LHa-IS1, Figure 3a) is -0.44 eV and ΔG is 0.22 eV (at 298.15 K, $P_{\text{CO}} = 0.01$ atm, $P_{\text{CO}}/P_{\text{O}_2} = 1:20$). The variation of ΔG from LH-MS1 also suggests that the adsorbed CO would be reactive for subsequent reactions [55,76]. In LHa-IS1, Au is $+0.61$ |e| charged to interact with 3 N at a B-vacancy of *h*-BN, O and C of peroxide intermediate (OOCO) and the newly adsorbed CO. The calculated C = O stretching frequency in OOCO is blue shifted from 1748 cm⁻¹ to 1811 cm⁻¹, while that in CO is also blue shifted to 2125 cm⁻¹. These correlate well with the charge on Au. OCOO dissociation and subsequent reactions was then investigated. As aforementioned, OCOO will dissociate to form CO₂ and AuO with an energy barrier of 0.51 eV. The calculated energy barrier for OCOO dissociation in LHa-IS1 is 0.44 eV and is lowered by 0.07 eV. One may raise concern with the CO desorption during or prior to OCOO dissociation. The O(CO)-Au distance is decreased slightly from 2.09 (in LHa-IS1) to 2.05 Å in the corresponding TS (LHa-TS1, Figure 3b) and is further decreased to 2.02 Å in the product (LHa-MS1, Figure 3c) that is a coadsorption structure of atomic O and CO with a CO₂ interacting electrostatically with O(Au). The continuous decrease in the Au-C distance during this process indicates that OCOO dissociation may not drive desorption of CO but stabilize it instead. After desorption of CO₂ in LHa-MS1, further reactions may take place between coadsorbed CO and O in LHa-MS2 (Figure 3d). As mediated by Au, the coadsorbed O and CO combine together by crossing a TS (LHa-MS2, Figure 3e) with a reaction barrier of 0.01 eV and free energy barrier of 0.05 eV, to form another CO₂ (LHa-FS1, Figure 3f). The calculated (free) energy barriers on the newly proposed pathway for the evolution of LHa-IS1 are much lower than those on the rLH pathway (Figures 2j and 3j). The decreased reaction barrier provides direct evidence for the promotion effect of CO in OCOO dissociation.

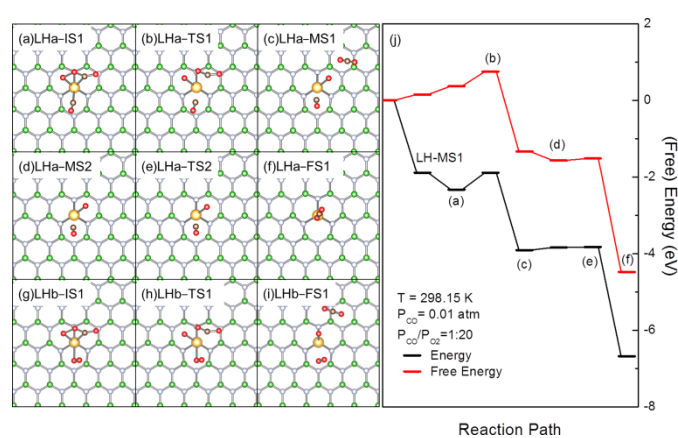


Figure 3. Optimized structures of the reaction species involved, including reaction intermediates, transition states and products (a–i), and (free) energy profiles (j) for CO oxidation over AuBN with the LHa and LHb pathways initiated with the coadsorption of CO or O₂ with LH-MS1. In (a–i), the B, N, C and Au atoms are in green, light blue, brown and gold, respectively. In (j), the bracketed letters correspond to the structures shown in (a–i).

Coadsorption of O_2 with OCOO leads to the formation of LHb-IS1 (Figure 3g). The calculated E_{ad} of O_2 is -0.15 eV and the corresponding ΔG is 0.41 eV. The weak adsorption of O_2 can be attributed to the positive charged nature of the Au center in LH-MS1. The calculated O_2 dissociation energy barrier and free energy barrier on AuBN is 1.79 and 1.78 eV, respectively, so AuBN is not capable of O_2 dissociation. The reaction goes through a TS (LHb-TS1, Figure 3h) with a barrier of 1.00 eV and the free energy barrier of 0.92 eV, forming physisorbed O_2 and CO_2 around AuO (LHb-FS1, Figure 3i). As the OCOO dissociation barrier is increased to be much higher than E_{ad} (ΔG) for O_2 adsorption, O_2 desorption may take place with high priority and may not impact OCOO dissociation.

Apart from promoting the dissociation of OCOO, the coadsorbed CO may also react with OCOO. In LHc-IS1 (Figure 4a), Au is highly positively charged ($+0.61$ |e|), O bound to Au is negatively charged (-0.20 |e|) and C(CO) is also positively charged ($+0.19$ |e|). CO may interact electrostatically with O(Au) to reach a TS (LHc-TS1, Figure 4b) with energy and free energy barriers of 0.18 and 0.64 eV, respectively, for the formation of OCOOCO intermediate (LHc-MS1, Figure 4c) that was previously proposed on a three-molecule ER(ER3) type pathway for CO oxidation [53]. In LHc-TS1, OCOO is distorted to facilitate the O(Au)-C(CO) interaction, with the increase in the O(Au)-Au and decrease in O(Au)-C(CO) distance, showing the tendency for the formation of the Au-C bond at the expense of the Au-O bond. The corresponding energy and free energy barriers are 0.18 and 0.64 eV, respectively. As a result of these interactions, CO is inserted into the O-Au bond forming a planar OCOOCO intermediate nearly vertical to one of the interfacial Au-N bonds (LHc-MS1). Due to the instability of the peroxo O-O bond, LHc-MS1 may undergo dissociation by breaking the O-O and Au-C bonds in the corresponding TS (LHc-TS2, Figure 4d) with energy and free energy barriers of 0.38 and 0.27 eV, respectively, to form 2 CO_2 physisorbed at AuBN (LHc-FS1, Figure 4e).

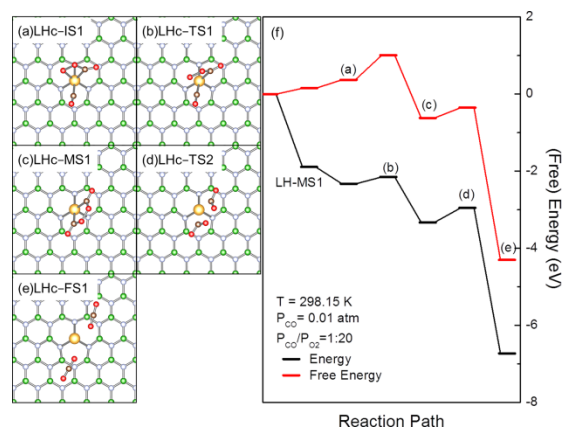


Figure 4. Optimized structures of the reaction species involved, including reaction intermediates, transition states and products (a–e), and (free) energy profiles (f) for CO oxidation over AuBN, with the LHc pathway initiated with the coadsorption of CO with LH-MS1. In (a–e), the B, N, C and Au atoms are in green, light blue, brown and gold, respectively. In (f), the bracketed letters correspond to the structures shown in (a–e).

As Au in LHb-MS1 is also pentacoordinated, coadsorption of CO or O_2 may also take place. The impact of coadsorbed CO and O_2 for the further evolution of LHc-MS1 was also investigated. Both CO and O_2 cannot react with OCOOCO intermediate, they will retain and adsorb on AuBN after the dissociation of LHc-MS1. As Au is already positively charged in LHc-MS1, the calculated E_{ad} for CO and O_2 coadsorption are -0.21 and -0.09 eV, respectively, while ΔG are 0.52 and 0.46 eV, respectively. This is similar to the aforementioned coadsorption of CO or O_2 with OOCO. With the coadsorption of reactants, the energy and free energy barriers for OCOOCO dissociation change to 0.49 and 0.28 eV, respectively, for CO and 0.19 and 0.15 eV, respectively, for O_2 . The variation of the

reaction barrier with coadsorption of CO or O₂ once again provides direct evidence for the interference of coadsorbed CO or O₂ to the evolution of reaction species and CO conversion.

AuO is another important intermediate on the rLH pathway for CO oxidation. AuO is formed by the dissociation of LH-MS1 and may be consumed by direct reaction with gaseous CO [39]. In AuO, O is negatively charged ($-0.30 |e|$). Previously, such negatively charged O-containing species in mesoporous carbon materials were proposed as reactive CO₂ binding sites [84]. The calculated CO₂ E_{ad} for CO₂ physisorption on AuO (LHd-IS1, Figure 5a) is -0.07 eV and the corresponding ΔG is 0.51 eV. These are in reasonable agreement with Pd, Fe and Au SACs on graphene [31,55,56]. In LHd-IS1, both the C-O bonds are nearly vertical to C(CO₂)-O(Au) direction. Following the O(Au)-C(CO₂) electrostatic interaction, CO₂ moves to O(Au) by crossing a TS (LHd-TS1, Figure 5b) with a barrier of 0.18 eV and free energy barrier of 0.34 eV for the formation of carbonate (CO₃, LHd-MS1, Figure 5c). The O(CO)-C-O angle also changes from 85° to $\sim 94^\circ$, demonstrating that CO₂ is activated to interact with both O(Au) and Au in this process. The interaction is further enhanced in LHd-MS1, as the O(C)-C-O(Au) is distorted to be $\sim 120^\circ$. Au in AuBN is also oxidized during this process, as the charge on Au changes from $0.56 |e|$ to $0.64 |e|$ in LHd-MS1. The energy and free energy change for the formation of CO₃ are -0.98 and -1.19 eV, respectively, while the calculated energy and free energy barriers for CO₃ dissociation are 1.38 and 1.28 eV, respectively. Therefore, the direct dissociation of CO₃ is rather demanding over AuBN. In this sense, CO₃ formation is plausible by the reaction of gaseous CO₂ with AuO. This pathway also connects the evolution of OCOO to thermodynamically more plausible CO₃ species and solves the concern for formation and evolution of CO₃ species in CO oxidation on SACs [73–75,85]. We then moved on to investigate the potential coadsorption with CO and whether CO may promote the conversion of CO₃ [56]. The CO coadsorption leads to the formation of LHd-MS2 (Figure 5d). The calculated CO E_{ad} and ΔG are -0.42 and 0.16 eV, respectively. The small positive change of ΔG suggests coadsorbed CO would be highly reactive [55,76]. According to the charge distribution, the positively charged C(CO) may move to react with negatively charged O(Au) at the interface by crossing the TS (LHd-TS2, Figure 5e) with the energy barrier and free energy barriers of 0.36 and 0.34 eV, respectively, to reach the intermediate (LHd-MS3, Figure 5f), where CO is inserted into an Au-O bond forming a planar C₂O₄ species with an ultra-long C-O bond of 1.45 Å, which introduces instability into this structure. LHd-MS3 may further evolve by breaking the ultra-long C-O bond and charge reorganization to reach a TS (LHd-TS3, Figure 5g) with energy and free energy barriers of 0.26 and 0.19 eV, respectively. In this way, LHc-MS3 dissociates into 2 physisorbed CO₂ adsorbed on AuBN (LHd-MS4, Figure 5h). During this process, 2 C(O) were oxidized and charges were transferred to Au. As aforementioned, the coadsorbed CO may also act as a spectator in CO₃ dissociation. For comparison, the dissociation of CO₃ in LHc-MS2 in this way was also investigated. In this process, the reaction proceeds through a TS (LHc-TS4, Figure 5i) with calculated energy and free energy barriers of 1.85 and 1.59 eV, respectively, to reach the product with a coadsorption of atomic oxygen, CO and a physisorbed CO₂ around the Au center (LHa-MS1, Figure 3c). The barriers at LHd-TS4 are much higher compared with the direct dissociation of CO₃ and the reaction of coadsorbed CO with CO₃, demonstrating the influence of coadsorbed reactants to the evolution of reaction species and the CO conversion.

To this end, the coadsorbed CO, O₂ or CO₂ may lead to the formation of new reaction species with different reactivity and their evolution through pathways complementary to the rLH pathway for CO oxidation. Specifically, the coadsorbed CO or O₂ may promote the evolution of reaction intermediates, considering the CO promoted the dissociation of OCOO (LHa, Figure 3) and O₂ promoted the dissociation of OCOOCO. Or, they would react to form new reaction species, such as the formation of OCOOCO by the reaction of CO with OCOO (LHb, Figure 4) and the formation of C₂O₄ by the reaction of CO with CO₃ (LHd, Figure 5), initiating new pathways for CO oxidation. Considering the limited E_{ad} and ΔG of these coadsorbed species, their formation would be strongly interfered by reaction

conditions. At low partial pressure and high temperature, coadsorption of reactants would be vanished and the reaction may mainly proceed with the rLH pathway (Figure 2) with the formation and dissociation of peroxide intermediate and a direct reaction with gaseous CO. High partial pressure and low temperature may benefit the formation of coadsorbed structures of different reactivity to enable the switching of the reaction pathway. This effect would be significant for the LHb (Figure 3) pathway and promotes the CO-assisted dissociation of OCOO, as well as the CO₃ formation and evolution initiated with the reaction of AuO with CO₂ (LHd, Figure 5). CO₃ is also an important reaction species, considering the strong exothermicity for formation and its reaction with coadsorbed CO, which makes the circumvention of the potentially sluggish reaction of gaseous CO with AuO possible [86].

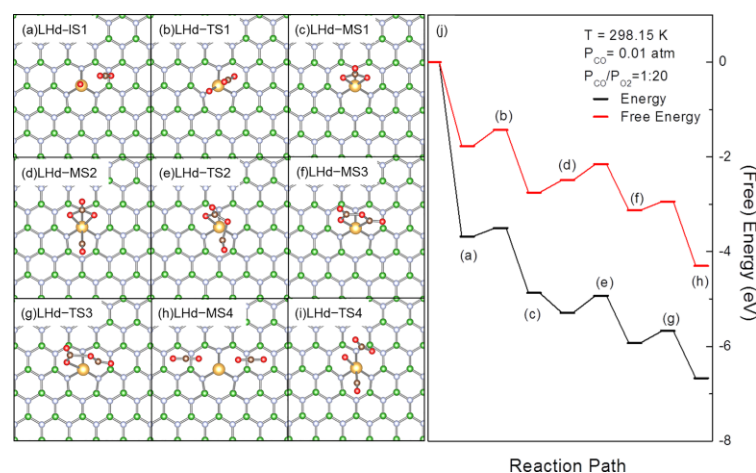


Figure 5. Optimized structures of the reaction species involved, including reaction intermediates, transition states and products (a–i), and (free) energy profiles (j) for CO oxidation over AuBN with the LHd pathway initiated with the coadsorption of CO with LH–MS1. In (a–i), the B, N, C and Au atoms are in green, light blue, brown and gold, respectively. In (j), the bracketed letters correspond to the structures shown in (a–h).

3.4. Comparison with Other Alternative Pathways

We have discussed CO oxidation over AuBN through the rLH pathway and its variants and would now move further to compare these with the remaining. An ER type pathway is initiated with the adsorption and activation of one of the reactants for subsequent reaction with the other gaseous reactants. Theoretically, several ER type pathways were proposed for CO oxidation over SACs, including one molecular ER pathway (ER1), where O₂ or CO should be activated at the metal center to react with gaseous reactant for the formation of CO₂ and surface O species [87], two molecular ER (ER2) pathways where gaseous CO react with activated O₂ forming CO₃ as a stable intermediate [88] and an ER3 pathway that can be identified with the OCOOCO intermediate formed by the reaction of gaseous O₂ with two pre-adsorbed CO [53], etc. These pathways all initiate with the van de Waals complexes formed between surface species and the gaseous reactants. According to the thermodynamics data (Figure 1j), AuCO is the most plausible surface species with AuO₂ + CO ranking the second. The van de Waals complexes formed between preadsorbed CO or O₂ with gaseous reactants, such as AuO₂ + CO(g), Au(CO)₂ + O₂(g), etc., are less plausible as compared with the corresponding surface species, such as AuO₂ + CO, etc., while Au(CO)₂ + O₂ is unstable and O₂ may desorb during structure optimization. The superior stability of reaction species on LH type pathways over those van de Waals complexes were previously reported for in CO oxidation over other SACs, where the relative stability among these reaction species were proposed to account for the dominant role of the rLH pathway in the CO oxidation [55,56]. Further to these, the charge transfer from activated O₂ to CO is required for the formation of CO₃ intermediate on the ER2

pathway, and a reaction of this kind is always accompanied with high reaction barriers. The ground state of $\text{Au}(\text{CO})_2 + \text{O}_2(\text{g})$ is of triplet symmetry, and the spin is localized on O_2 , making the formation of OCOOCO species of singlet symmetry spin-forbidden. Therefore, the reactions along ER2 and ER3 pathways on AuBN would be rather demanding as compared to those on LH type pathways. As only O_2 was activated on the ER1 pathway, the reaction is between activated O_2 and gaseous CO and the calculated energy and free energy barriers for the formation of first CO_2 are 0.71 and 0.84 eV, respectively, and are much higher as compared with those on the LH type pathways with the involvement of Au.

We fell back to consider the potential formation of the reaction species on ER type pathways and compared them with those on the rLH pathway and newly proposed variants. It is interesting to note that all reaction species, such as CO_3 , OCOOCO , etc., were already included on newly proposed variants of the rLH pathway. Furthermore, the thermostability of some reaction species on ER pathways are lower as compared with corresponding species on LH type pathways, demonstrating that their evolution to those stable species on LH type pathways by adsorbate adsorption/desorption or exchange would be thermodynamics driven. Therefore, their evolution to and on the LH-type pathways would be more reasonable, and would be strongly interfered with by the reaction conditions.

4. Conclusions

The reaction condition-dependent catalytic performance of a SAC has long been realized, but seldom investigated before. We investigated CO oxidation pathways over SACs in reaction conditions, using AuBN as a model with extensive first-principles-based calculations. We showed that the adsorption of reactants, namely CO, O_2 and CO_2 , and their coadsorption with reaction species on AuBN, would be condition dependent, leading to various reaction species with different reactivity and impact to the CO conversion. New pathways originating from these reaction species, complementary to rLH pathway, were proposed and may account for the CO conversion at the corresponding conditions. Specifically, the rLH pathway with CO-mediated activation of O_2 and the dissociation of the cyclic peroxide intermediate followed by the Eley–Rideal type reduction is dominant at high temperatures, while the coadsorbed CO-mediated dissociation of peroxide intermediate becomes plausible when coadsorption is allowed at low temperatures and high CO partial pressures. Carbonate species would also form in existence of CO_2 and would react with coadsorbed CO, promoting the CO oxidation. The pathways were currently proposed to investigate CO oxidation on AuBN, but can be delivered to other SACs by further integration with other alternatives pathways that require features not available on AuBN, such as the Mars–van–Krevelen type pathways and those require the involvement of the support. The findings highlight the condition-dependent CO oxidation over SACs may originate from the thermostability of reaction species in detailed conditions and may help to rationalize the current understanding to the superior catalytic performance of SACs.

Author Contributions: X.L. designed the research and wrote the manuscript. X.Z. performed the first-principles-based calculations and analyzed the results. X.Z. is responsible for the results presented. X.L. and C.M. provided the resources, commented on the results and proofed the manuscript. All authors have read and agreed to the published version of the manuscript.

Funding: This work was supported by NSFC (21771029, 11811530631, 21573034, 21373036 and 21103015).

Institutional Review Board Statement: Not applicable.

Informed Consent Statement: Not applicable.

Conflicts of Interest: The authors declare no conflict of interest.

References

1. Wang, A.; Li, J.; Zhang, T. Heterogeneous single-atom catalysis. *Nat. Rev. Chem.* **2018**, *2*, 65–81. [[CrossRef](#)]
2. Liu, J.Y. Catalysis by Supported Single Metal Atoms. *ACS Catal.* **2017**, *7*, 34–59. [[CrossRef](#)]
3. Cui, X.J.; Li, W.; Ryabchuk, P.; Junge, K.; Beller, M. Bridging homogeneous and heterogeneous catalysis by heterogeneous single-metal-site catalysts. *Nat. Catal.* **2018**, *1*, 385–397. [[CrossRef](#)]
4. Samantaray, M.K.; D'Eia, V.; Pump, E.; Falivene, L.; Harb, M.; Chikh, S.O.; Cavallo, L.; Basset, J.M. The Comparison between Single Atom Catalysis and Surface Organometallic Catalysis. *Chem. Rev.* **2020**, *120*, 734–813. [[CrossRef](#)] [[PubMed](#)]
5. Zhou, X.; Shen, Q.; Yuan, K.; Yang, W.; Chen, Q.; Geng, Z.; Zhang, J.; Shao, X.; Chen, W.; Xu, G.; et al. Unraveling Charge State of Supported Au Single-Atoms during CO Oxidation. *J. Am. Chem. Soc.* **2018**, *140*, 554–557. [[CrossRef](#)]
6. Kaatz, F.H.; Murzin, D.Y.; Bultheel, A. Coordination-Dependent Kinetics in the Catalysis of Gold Nanoclusters. *ACS Catal.* **2021**, *11*, 9073–9085. [[CrossRef](#)]
7. Piccolo, L. Restructuring effects of the chemical environment in metal nanocatalysis and single-atom catalysis. *Catal. Today* **2020**, *373*, 80–97. [[CrossRef](#)]
8. Li, Y.; Li, S.K.; Baumer, M.; Moskaleva, L.V. Transient Au-CO Complexes Promote the Activity of an Inverse Ceria/Gold Catalyst: An Insight from Ab Initio Molecular Dynamics. *J. Phys. Chem. C* **2021**, *125*, 26406–26417. [[CrossRef](#)]
9. Wang, Y.G.; Yoon, Y.; Glezakou, V.A.; Li, J.; Rousseau, R. The Role of Reducible Oxide-Metal Cluster Charge Transfer in Catalytic Processes: New Insights on the Catalytic Mechanism of CO Oxidation on Au/TiO₂ from ab Initio Molecular Dynamics. *J. Am. Chem. Soc.* **2013**, *135*, 10673–10683. [[CrossRef](#)]
10. Wang, Y.G.; Mei, D.H.; Glezakou, V.A.; Li, J.; Rousseau, R. Dynamic formation of single-atom catalytic active sites on ceria-supported gold nanoparticles. *Nat. Commun.* **2015**, *6*, 8. [[CrossRef](#)]
11. Liu, J.C.; Wang, Y.G.; Li, J. Toward Rational Design of Oxide-Supported Single-Atom Catalysts: Atomic Dispersion of Gold on Ceria. *J. Am. Chem. Soc.* **2017**, *139*, 6190–6199. [[CrossRef](#)] [[PubMed](#)]
12. He, Y.; Liu, J.C.; Luo, L.L.; Wang, Y.G.; Zhu, J.F.; Du, Y.G.; Li, J.; Mao, S.X.; Wang, C.M. Size-dependent dynamic structures of supported gold nanoparticles in CO oxidation reaction condition. *Proc. Natl. Acad. Sci. USA* **2018**, *115*, 7700–7705. [[CrossRef](#)] [[PubMed](#)]
13. Mandal, K.; Gu, Y.T.; Westendorff, K.S.; Li, S.C.; Pihl, J.A.; Grabow, L.C.; Epling, W.S.; Paolucci, C. Condition-Dependent Pd Speciation and NO Adsorption in Pd/Zeolites. *ACS Catal.* **2020**, *10*, 12801–12818. [[CrossRef](#)]
14. Ouyang, R.H.; Liu, J.X.; Li, W.X. Atomistic Theory of Ostwald Ripening and Disintegration of Supported Metal Particles under Reaction Conditions. *J. Am. Chem. Soc.* **2013**, *135*, 1760–1771. [[CrossRef](#)]
15. Stamatakis, M.; Christiansen, M.A.; Vlachos, D.G.; Mpourmpakis, G. Multiscale Modeling Reveals Poisoning Mechanisms of MgO-Supported Au Clusters in CO Oxidation. *Nano Lett.* **2012**, *12*, 3621–3626. [[CrossRef](#)]
16. Negreiros, F.R.; Camellone, M.F.; Fabris, S. Effects of Thermal Fluctuations on the Hydroxylation and Reduction of Ceria Surfaces by Molecular H₂. *J. Phys. Chem. C* **2015**, *119*, 21567–21573. [[CrossRef](#)]
17. Ghosh, P.; Camellone, M.F.; Fabris, S. Fluxionality of Au Clusters at Ceria Surfaces during CO Oxidation: Relationships among Reactivity, Size, Cohesion, and Surface Defects from DFT Simulations. *J. Phys. Chem. Lett.* **2013**, *4*, 2256–2263. [[CrossRef](#)]
18. Liu, J.C.; Tang, Y.; Chang, C.R.; Wang, Y.G.; Li, J. Mechanistic Insights into Propene Epoxidation with O₂-H₂O Mixture on Au-7/ α -Al₂O₃: A Hydroproxyl Pathway from ab Initio Molecular Dynamics Simulations. *ACS Catal.* **2016**, *6*, 2525–2535. [[CrossRef](#)]
19. Wang, Y.G.; Cantu, D.C.; Lee, M.S.; Li, J.; Glezakou, V.A.; Rousseau, R. CO Oxidation on Au/TiO₂: Condition-Dependent Active Sites and Mechanistic Pathways. *J. Am. Chem. Soc.* **2016**, *138*, 10467–10476. [[CrossRef](#)]
20. Ding, K.; Gulec, A.; Johnson, A.M.; Schweitzer, N.M.; Stucky, G.D.; Marks, L.D.; Stair, P.C. Identification of active sites in CO oxidation and water-gas shift over supported Pt catalysts. *Science* **2015**, *350*, 189–192. [[CrossRef](#)]
21. Liu, K.; Wang, A.Q.; Zhang, T. Recent Advances in Preferential Oxidation of CO Reaction over Platinum Group Metal Catalysts. *ACS Catal.* **2012**, *2*, 1165–1178. [[CrossRef](#)]
22. Beniya, A.; Higashi, S. Towards dense single-atom catalysts for future automotive applications. *Nat. Catal.* **2019**, *2*, 590–602. [[CrossRef](#)]
23. Freund, H.J.; Meijer, G.; Scheffler, M.; Schlogl, R.; Wolf, M. CO Oxidation as a Prototypical Reaction for Heterogeneous Processes. *Angew. Chem.-Int. Edit.* **2011**, *50*, 10064–10094. [[CrossRef](#)] [[PubMed](#)]
24. Qiao, B.; Wang, A.; Yang, X.; Allard, L.F.; Jiang, Z.; Cui, Y.; Liu, J.; Li, J.; Zhang, T. Single-Atom catalysis of CO oxidation using Pt-1/FeOx. *Nat. Chem.* **2011**, *3*, 634–641. [[CrossRef](#)] [[PubMed](#)]
25. Haruta, M.; Kobayashi, T.; Sano, H.; Yamada, N. Novel Gold Catalysts for the Oxidation of Carbon-Monoxide at a Temperature Far Below 0-Degrees-C. *Chem. Lett.* **1987**, *16*, 405–408. [[CrossRef](#)]
26. Hutchings, G. A golden future. *Nat. Chem.* **2009**, *1*, 584. [[CrossRef](#)]
27. Flytzani-Stephanopoulos, M. Gold Atoms Stabilized on Various Supports Catalyze the Water-Gas Shift Reaction. *Acc. Chem. Res.* **2014**, *47*, 783–792. [[CrossRef](#)]
28. Yao, K.X.; Liu, X.; Zhao, L.; Zeng, H.C.; Han, Y. Site-specific growth of Au particles on ZnO nanopyramids under ultraviolet illumination. *Nanoscale* **2011**, *3*, 4195–4200. [[CrossRef](#)]
29. Wang, C.Y.; Yang, M.; Flytzani-Stephanopoulos, M. Single gold atoms stabilized on nanoscale metal oxide supports are catalytic active centers for various reactions. *AlChE J.* **2016**, *62*, 429–439. [[CrossRef](#)]

30. Gu, X.K.; Qiao, B.T.; Huang, C.Q.; Ding, W.C.; Sun, K.J.; Zhan, E.S.; Zhang, T.; Liu, J.Y.; Li, W.X. Supported Single Pt-1/Au-1 Atoms for Methanol Steam Reforming. *ACS Catal.* **2014**, *4*, 3886–3890. [[CrossRef](#)]
31. Liu, X.; Yang, Y.; Chu, M.; Duan, T.; Meng, C.; Han, Y. Defect Stabilized Gold Atoms on Graphene as Potential Catalysts for Ethylene Epoxidation: A First-principles Investigation. *Catal. Sci. Technol.* **2016**, *6*, 1632–1641. [[CrossRef](#)]
32. Chen, Z.; Chen, Y.J.; Chao, S.L.; Dong, X.B.; Chen, W.X.; Luo, J.; Liu, C.G.; Wang, D.S.; Chen, C.; Li, W.; et al. Single-Atom Au-I-N-3 Site for Acetylene Hydrochlorination Reaction. *ACS Catal.* **2020**, *10*, 1865–1870. [[CrossRef](#)]
33. Zhang, X.; Shi, H.; Xu, B.Q. Catalysis by gold: Isolated surface Au³⁺ ions are active sites for selective hydrogenation of 1,3-butadiene over Au/ZrO₂ catalysts. *Angew. Chem.-Int. Edit.* **2005**, *44*, 7132–7135. [[CrossRef](#)]
34. Wang, C.Y.; Garbarino, G.; Allard, L.F.; Wilson, F.; Busca, G.; Flytzani-Stephanopoulos, M. Low-Temperature Dehydrogenation of Ethanol on Atomically Dispersed Gold Supported on ZnZrOx. *ACS Catal.* **2016**, *6*, 210–218. [[CrossRef](#)]
35. Mochizuki, C.; Inomata, Y.; Yasumura, S.; Lin, M.; Taketoshi, A.; Honma, T.; Sakaguchi, N.; Haruta, M.; Shimizu, K.-I.; Ishida, T.; et al. Defective NiO as a Stabilizer for Au Single-Atom Catalysts. *ACS Catal.* **2022**, *12*, 6149–6158. [[CrossRef](#)]
36. Kropp, T.; Lu, Z.; Li, Z.; Chin, Y.-H.C.; Mavrikakis, M. Anionic Single-Atom Catalysts for CO Oxidation: Support-Independent Activity at Low Temperatures. *ACS Catal.* **2019**, *9*, 1595–1604. [[CrossRef](#)]
37. Gao, M.; Lyalin, A.; Taketsugu, T. CO oxidation on h-BN supported Au atom. *J. Chem. Phys.* **2013**, *138*, 034701. [[CrossRef](#)] [[PubMed](#)]
38. Qiao, B.T.; Liu, J.X.; Wang, Y.G.; Lin, Q.Q.; Liu, X.Y.; Wang, A.Q.; Li, J.; Zhang, T.; Liu, J.Y. Highly Efficient Catalysis of Preferential Oxidation of CO in H-2-Rich Stream by Gold Single-Atom Catalysts. *ACS Catal.* **2015**, *5*, 6249–6254. [[CrossRef](#)]
39. Lu, Y.H.; Zhou, M.; Zhang, C.; Feng, Y.P. Metal-Embedded Graphene: A Possible Catalyst with High Activity. *J. Phys. Chem. C* **2009**, *113*, 20156–20160. [[CrossRef](#)]
40. Weng, Q.H.; Wang, X.B.; Wang, X.; Bando, Y.; Golberg, D. Functionalized hexagonal boron nitride nanomaterials: Emerging properties and applications. *Chem. Soc. Rev.* **2016**, *45*, 3989–4012. [[CrossRef](#)]
41. Zhu, W.S.; Wu, Z.L.; Foo, G.S.; Gao, X.; Zhou, M.X.; Liu, B.; Veith, G.M.; Wu, P.W.; Browning, K.L.; Lee, H.N.; et al. Taming interfacial electronic properties of platinum nanoparticles on vacancy-abundant boron nitride nanosheets for enhanced catalysis. *Nat. Commun.* **2017**, *8*, 15291. [[CrossRef](#)] [[PubMed](#)]
42. Zheng, Z.Y.; Cox, M.; Li, B. Surface modification of hexagonal boron nitride nanomaterials: A review. *J. Mater. Sci.* **2018**, *53*, 66–99. [[CrossRef](#)]
43. Fang, C.; An, W. Single-Metal-Atom site with high-spin state embedded in defective BN nanosheet promotes electrocatalytic nitrogen reduction. *Nano Res.* **2021**, *14*, 4211–4219. [[CrossRef](#)]
44. Fan, M.M.; Jimenez, J.D.; Shirodkar, S.N.; Wu, J.J.; Chen, S.M.; Song, L.; Royko, M.M.; Zhang, J.J.; Guo, H.; Cui, J.W.; et al. Atomic Ru Immobilized on Porous h-BN through Simple Vacuum Filtration for Highly Active and Selective CO₂ Methanation. *ACS Catal.* **2019**, *9*, 10077–10086. [[CrossRef](#)]
45. Zhang, W.; Fu, Q.; Luo, Q.; Sheng, L.; Yang, J. Understanding Single-Atom Catalysis in View of Theory. *JACS Au* **2021**, *1*, 2130–2145. [[CrossRef](#)]
46. Dong, J.H.; Gao, L.J.; Fu, Q. Hexagonal Boron Nitride Meeting Metal: A New Opportunity and Territory in Heterogeneous Catalysis. *J. Phys. Chem. Lett.* **2021**, *12*, 9608–9619. [[CrossRef](#)]
47. Zhao, J.X.; Chen, Z.F. Single Mo Atom Supported on Defective Boron Nitride Monolayer as an Efficient Electrocatalyst for Nitrogen Fixation: A Computational Study. *J. Am. Chem. Soc.* **2017**, *139*, 12480–12487. [[CrossRef](#)]
48. Gao, S.S.; Ma, Z.J.; Xiao, C.W.; Cui, Z.T.; Du, W.; Sun, X.Q.; Li, Q.H.; Sa, R.J.; Sun, C.H. TM₃ (TM = V, Fe, Mo, W) single-cluster catalyst confined on porous BN for electrocatalytic nitrogen reduction. *J. Mater. Sci. Technol.* **2022**, *108*, 46–53. [[CrossRef](#)]
49. Zhang, Y.F.; Zeng, Z.Y.; Li, H. Design of 3d transition metal anchored B₅N₃ catalysts for electrochemical CO₂ reduction to methane. *J. Mater. Chem. A* **2022**, *10*, 9737–9745. [[CrossRef](#)]
50. Hu, G.X.; Wu, Z.L.; Dai, S.; Jiang, D.E. Interface Engineering of Earth-Abundant Transition Metals Using Boron Nitride for Selective Electroreduction of CO₂. *ACS Appl. Mater. Interfaces* **2018**, *10*, 6694–6700. [[CrossRef](#)]
51. Li, Z.; Wei, W.; Li, H.; Li, S.; Leng, L.; Zhang, M.; Horton, J.H.; Wang, D.; Sun, W.; Guo, C.; et al. Low-Temperature Synthesis of Single Palladium Atoms Supported on Defective Hexagonal Boron Nitride Nanosheet for Chemoselective Hydrogenation of Cinnamaldehyde. *ACS Nano* **2021**, *15*, 10175–10184. [[CrossRef](#)] [[PubMed](#)]
52. Xiong, C.; Dai, S.; Wu, Z.; Jiang, D.-e. Single Atoms Anchored in Hexagonal Boron Nitride for Propane Dehydrogenation from First Principles. *ChemCatChem* **2022**, *14*, e202200133. [[CrossRef](#)]
53. Mao, K.; Li, L.; Zhang, W.; Pei, Y.; Zeng, X.C.; Wu, X.; Yang, J. A Theoretical Study of Single-Atom Catalysis of CO Oxidation Using Au Embedded 2D h-BN Monolayer: A CO-Promoted O-2 Activation. *Sci. Rep.* **2014**, *4*, 5441. [[CrossRef](#)] [[PubMed](#)]
54. Zhang, M.H.; Du, J.B.; Chen, Y.F. Single Cu atom supported on modified h-BN monolayer as n-p codoped catalyst for CO oxidation: A computational study. *Catal. Today* **2021**, *368*, 148–160. [[CrossRef](#)]
55. Liu, X.; Xu, M.; Wan, L.; Zhu, H.; Yao, K.; Linguerrri, R.; Chambaud, G.; Han, Y.; Meng, C. Superior Catalytic Performance of Atomically Dispersed Palladium on Graphene in CO Oxidation. *ACS Catal.* **2020**, *10*, 3084–3093. [[CrossRef](#)]
56. Zhu, J.; Feng, X.; Liu, X.; Zhang, X.; Wu, Y.; Zhu, H.; Yang, Y.; Duan, T.; Sui, Y.; Han, Y.; et al. The formation and evolution of carbonate species in CO oxidation over mono-dispersed Fe on graphene. *Phys. Chem. Chem. Phys.* **2021**, *23*, 10509–10517. [[CrossRef](#)]

57. Perdew, J.P.; Burke, K.; Ernzerhof, M. Generalized gradient approximation made simple. *Phys. Rev. Lett.* **1996**, *77*, 3865–3868. [[CrossRef](#)]
58. Delley, B. Hardness conserving semilocal pseudopotentials. *Phys. Rev. B* **2002**, *66*, 155125. [[CrossRef](#)]
59. Inada, Y.; Orita, H. Efficiency of numerical basis sets for predicting the binding energies of hydrogen bonded complexes: Evidence of small basis set superposition error compared to Gaussian basis sets. *J. Comput. Chem.* **2008**, *29*, 225–232. [[CrossRef](#)]
60. Delley, B. An All-Electron Numerical-Method for Solving the Local Density Functional for Polyatomic-Molecules. *J. Chem. Phys.* **1990**, *92*, 508–517. [[CrossRef](#)]
61. Delley, B. From molecules to solids with the DMol(3) approach. *J. Chem. Phys.* **2000**, *113*, 7756–7764. [[CrossRef](#)]
62. Monkhorst, H.J.; Pack, J.D. Special Points for Brillouin-Zone Integrations. *Phys. Rev. B* **1976**, *13*, 5188–5192. [[CrossRef](#)]
63. Govind, N.; Petersen, M.; Fitzgerald, G.; King-Smith, D.; Andzelm, J. A generalized synchronous transit method for transition state location. *Comput. Mater. Sci.* **2003**, *28*, 250–258. [[CrossRef](#)]
64. Hirshfeld, F.L. Bonded-Atom Fragments for Describing Molecular Charge-Densities. *Theor. Chim. Acta* **1977**, *44*, 129–138. [[CrossRef](#)]
65. Gajdos, M.; Eichler, A.; Hafner, J. CO adsorption on close-packed transition and noble metal surfaces: Trends from ab initio calculations. *J. Phys.-Condes. Matter* **2004**, *16*, 1141–1164. [[CrossRef](#)]
66. Castro Neto, A.H.; Guinea, F.; Peres, N.M.R.; Novoselov, K.S.; Geim, A.K. The electronic properties of graphene. *Rev. Mod. Phys.* **2009**, *81*, 109–162. [[CrossRef](#)]
67. Wang, C.L.; Gu, X.K.; Yan, H.; Lin, Y.; Li, J.J.; Liu, D.D.; Li, W.X.; Lu, J.L. Water-Mediated Mars-Van Krevelen Mechanism for CO Oxidation on Ceria-Supported Single-Atom Pt-1 Catalyst. *ACS Catal.* **2017**, *7*, 887–891. [[CrossRef](#)]
68. Bertoldi, D.S.; Ramos, S.B.; Guillermot, A.F. Interrelations between EOS parameters and cohesive energy of transition metals: Thermostatistical approach, ab initio calculations and analysis of “universality” features. *J. Phys. Chem. Solids* **2017**, *107*, 93–99. [[CrossRef](#)]
69. Chan, B.; Yim, W.L. Accurate Computation of Cohesive Energies for Small to Medium-Sized Gold Clusters. *J. Chem. Theory Comput.* **2013**, *9*, 1964–1970. [[CrossRef](#)]
70. Zhang, Y.S.; Liu, J.X.; Qian, K.; Jia, A.P.; Li, D.; Shi, L.; Hu, J.; Zhu, J.F.; Huang, W.X. Structure Sensitivity of Au-TiO₂ Strong Metal-Support Interactions. *Angew. Chem.-Int. Edit.* **2021**, *60*, 12074–12081. [[CrossRef](#)]
71. Kovalskii, A.M.; Volkov, I.N.; Evdokimenko, N.D.; Tkachenko, O.P.; Leybo, D.V.; Chepkasov, I.V.; Popov, Z.I.; Matveev, A.T.; Manakhov, A.; Permyakova, E.S.; et al. Hexagonal BN- and BNO-supported Au and Pt nanocatalysts in carbon monoxide oxidation and carbon dioxide hydrogenation reactions. *Appl. Catal. B-Environ.* **2022**, *303*, 16. [[CrossRef](#)]
72. Narula, C.K.; Stocks, G.M. Ab Initio Density Functional Calculations of Adsorption of Transition Metal Atoms on θ -Al₂O₃(010) Surface. *J. Phys. Chem. C* **2012**, *116*, 5628–5636. [[CrossRef](#)]
73. Moses-DeBusk, M.; Yoon, M.; Allard, L.F.; Mullins, D.R.; Wu, Z.; Yang, X.; Veith, G.; Stocks, G.M.; Narula, C.K. CO Oxidation on Supported Single Pt Atoms: Experimental and ab Initio Density Functional Studies of CO Interaction with Pt Atom on θ -Al₂O₃(010) Surface. *J. Am. Chem. Soc.* **2013**, *135*, 12634–12645. [[CrossRef](#)] [[PubMed](#)]
74. Narula, C.K.; Allard, L.F.; Wu, Z.L. Ab Initio Density Functional Calculations and Infra-Red Study of CO Interaction with Pd Atoms on theta-Al₂O₃ (010) Surface. *Sci. Rep.* **2017**, *7*, 8. [[CrossRef](#)] [[PubMed](#)]
75. Newton, M.A.; Ferri, D.; Smolentsev, G.; Marchionni, V.; Nachtegaal, M. Kinetic Studies of the Pt Carbonate-Mediated, Room-Temperature Oxidation of Carbon Monoxide by Oxygen over Pt/Al₂O₃ Using Combined, Time-Resolved XAFS, DRIFTS, and Mass Spectrometry. *J. Am. Chem. Soc.* **2016**, *138*, 13930–13940. [[CrossRef](#)] [[PubMed](#)]
76. Ammal, S.C.; Heyden, A. Water-Gas Shift Activity of Atomically Dispersed Cationic Platinum versus Metallic Platinum Clusters on Titania Supports. *ACS Catal.* **2017**, *7*, 301–309. [[CrossRef](#)]
77. Zhang, Z.L.; Zhu, Y.H.; Asakura, H.; Zhang, B.; Zhang, J.G.; Zhou, M.X.; Han, Y.; Tanaka, T.; Wang, A.Q.; Zhang, T.; et al. Thermally stable single atom Pt/m-Al₂O₃ for selective hydrogenation and CO oxidation. *Nat. Commun.* **2017**, *8*, 16100. [[CrossRef](#)]
78. Lu, Y.B.; Wang, J.M.; Yu, L.; Kovarik, L.; Zhang, X.W.; Hoffman, A.S.; Gallo, A.; Bare, S.R.; Sokaras, D.; Kroll, T.; et al. Identification of the active complex for CO oxidation over single-atom Ir-on-MgAl₂O₄ catalysts. *Nat. Catal.* **2019**, *2*, 149–156. [[CrossRef](#)]
79. Duan, Z.Y.; Henkelman, G. CO Oxidation on the Pd(111) Surface. *ACS Catal.* **2014**, *4*, 3435–3443. [[CrossRef](#)]
80. Piccinin, S.; Stamatakis, M. CO Oxidation on Pd(111): A First-Principles-Based Kinetic Monte Carlo Study. *ACS Catal.* **2014**, *4*, 2143–2152. [[CrossRef](#)]
81. Liu, X.; Zhu, H.; Linguerri, R.; Han, Y.; Chambaud, G.; Meng, C. Interfacial-Bonding-Regulated CO Oxidation over Pt Atoms Immobilized on Gas-Exfoliated Hexagonal Boron Nitride. *ChemistrySelect* **2017**, *2*, 9412–9419. [[CrossRef](#)]
82. Allian, A.D.; Takane, K.; Fujidala, K.L.; Hao, X.; Truex, T.J.; Cai, J.; Buda, C.; Neurock, M.; Iglesia, E. Chemisorption of CO and Mechanism of CO Oxidation on Supported Platinum Nanoclusters. *J. Am. Chem. Soc.* **2011**, *133*, 4498–4517. [[CrossRef](#)] [[PubMed](#)]
83. Kopecky, K.R.; Gomez, R.R. O-O Stretching Frequencies of Cyclic Peroxides—Stabilization of Peroxides by Alkoxy Substituents. *Can. J. Chem.-Rev. Can. Chim.* **1984**, *62*, 277–279. [[CrossRef](#)]
84. Zhao, Y.; Liu, X.; Yao, K.X.; Zhao, L.; Han, Y. Superior Capture of CO₂ Achieved by Introducing Extra-framework Cations into N-doped Microporous Carbon. *Chem. Mat.* **2012**, *24*, 4725–4734. [[CrossRef](#)]
85. Newton, M.A.; Ferri, D.; Smolentsev, G.; Marchionni, V.; Nachtegaal, M. Room-Temperature carbon monoxide oxidation by oxygen over Pt/Al₂O₃ mediated by reactive platinum carbonates. *Nat. Commun.* **2015**, *6*, 9675. [[CrossRef](#)]

86. Liu, B.; Li, W.P.; Song, W.Y.; Liu, J. Carbonate-Mediated Mars-van Krevelen mechanism for CO oxidation on cobalt-doped ceria catalysts: Facet-Dependence and coordination-dependence. *Phys. Chem. Chem. Phys.* **2018**, *20*, 16045–16059. [[CrossRef](#)]
87. Lin, S.; Ye, X.; Johnson, R.S.; Guo, H. First-Principles Investigations of Metal (Cu, Ag, Au, Pt, Rh, Pd, Fe, Co, and Ir) Doped Hexagonal Boron Nitride Nanosheets: Stability and Catalysis of CO Oxidation. *J. Phys. Chem. C* **2013**, *117*, 17319–17326. [[CrossRef](#)]
88. Li, Y.F.; Zhou, Z.; Yu, G.T.; Chen, W.; Chen, Z.F. CO Catalytic Oxidation on Iron-Embedded Graphene: Computational Quest for Low-Cost Nanocatalysts. *J. Phys. Chem. C* **2010**, *114*, 6250–6254. [[CrossRef](#)]